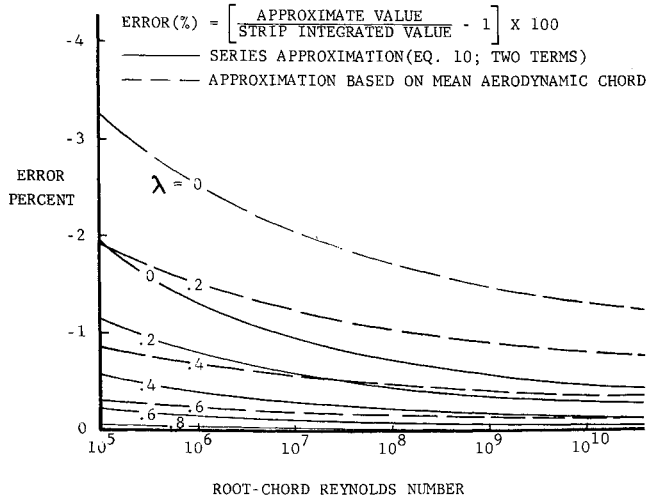

Fig. 2 Error in calculated skin friction as compared with strip integrated values.

term, we obtain

$$c_f = \frac{0.455}{(\log_{10}R_r)}\left\{1 + \frac{2.58}{(1+\lambda)\ln R_r} \times \left(\frac{1+\lambda}{2} + \frac{\lambda^2}{1-\lambda}\ln\lambda\right) + \frac{2.3091}{(\ln R_r)^2} \times \left[2\frac{\lambda^2}{1-\lambda^2}(1 - \ln\lambda)\ln\lambda + 1\right] + \ldots\right\} \quad (10)$$

If one places a further restriction on λ, it would be possible to make the series representation for c_f converge very quickly, such that only a few terms of Eq. (10) need be retained for good accuracy. If, in fact

$$\lambda \gg 1/R_r \quad (11)$$

the desired results are obtained. Again this places little restriction on λ.

From Eq. (10) it is seen that for rectangular planforms (i.e., $\lambda = 1$), c_f has the proper limit value. If $\lambda \to 0$, the relation obtained from Eq. (10) is exactly the same as obtained from the integral equation (7) for $\lambda = 0$ and is given by

$$c_{f_0} = \frac{0.455}{(\log_{10}R_r)^{2.58}}[1 + 1.29/\ln R_r + 2.3091/(\ln R_r)^2 + \ldots] \quad (12)$$

Strip integrated values for c_f were computed by using Eq. (7) with 100 strips/semispan. These values were used as a basis for comparison with both the approximate method developed herein [Eq. (10) or (12)] and the standard method using the wing mean aerodynamic chord. For Reynolds numbers in the range 10^5–10^{10}, the first two terms of Eq. (10) [or Eq. (12) for $\lambda = 0$] differ from strip integrated values by less than 2% for all taper ratios and in addition give better accuracy than the method utilizing the wing mean aerodynamic chord for all taper ratios except for $\lambda = 1$, where they are both exact (Fig. 2).

If three terms of Eq. (10) or Eq. (12) are used, the series approximation is nearly exact; differing from strip integrated values by only 0.4% for the worst case.

References

[1] Hopkins, E. J., "Some Effects of Planform Modification on the Skin Friction Drag," *AIAA Journal*, Vol. 2, No. 2, Feb. 1964, pp. 413–414.

[2] Barkhem, A., "Skin-Friction Formula for Tapered and Delta Wings," *Journal of Aircraft*, Vol. 6, No. 3, May-June 1969, p. 284.

[3] Schlichting, H., *Boundary Layer Theory*, 6th ed., McGraw-Hill, New York, 1968, p. 602.

Convergence-Proof of Discrete-Panel Wing Loading Theories

JOHN DEYOUNG*
University of Texas at Arlington, Arlington, Texas

Introduction

MANY wing surface loading theories use a finite elemental grid or lattice representation for the loading integral. As the lattice panel, such as a elemental horseshoe vortex, becomes small it induces velocity on its neighbor that approaches infinity. It had not been mathematically shown that this limit product of zero and infinity converges to the accurate finite loading.

The chordwise section-loading integral equation can be written in terms of vortices equally spaced along the wing chord. The summed vortex induced downwash at midpoints between the vortices give equations that satisfy the boundary condition of no flow through the wing. These result in N unknowns (of N load-vortices) and N equations which can be solved simultaneously.

A solution for any value of N has been derived which since 1967 has been proven accurate and useful for defining the chordwise loading curve from constant loading segments. Having exact mathematical solutions for a large number of simultaneous equations permits making accuracy checks of computers. Actually, the present solution was derived because a computer 15-term simultaneous equations solution appeared a little doubtful. This computer was proven to give erroneous loading values of up to 14% near the leading edge.

Analysis

The downwash at x_{em} due to a vortex at x_n is

$$w_{mn} = \Gamma_n/2\pi(x_{em} - x_n) \quad (1)$$

The distribution of chordwise vortices at the $\frac{1}{4}$ chord point of the equal length panels are shown in Fig. 1.

Let N be the number of panels. Then c/N is the length of each equal-length panel. The circulation at the quarter-chord of the nth panel is at the chord station

$$x_n = (n-1)(c/N) + (c/4N) = [n - \tfrac{3}{4}](c/N) \quad (2)$$

The $\frac{3}{4}$ chord of the nth panel is at the chord station

$$x_{em} = (m-1)(c/N) + (3c/4N) = (m - \tfrac{1}{4})(c/N) \quad (3)$$

With Eqs. (2) and (3), Eq. (1) becomes

$$(w_{mn}/V) = (N\Gamma_n/\pi cV)/(2m - 2n + 1) \quad (4)$$

Define e_n as

$$e_n = N\Gamma_n/\pi cV\alpha = \gamma_n/\pi V\alpha = -\Delta C_p/2\pi\alpha \quad (5)$$

Then the total downwash at chord station m is the summation of all the vortices. The flow angle that satisfies the boundary condition of no flow through the wing is from Eq. (4) given by

$$(\alpha_m/\alpha) = \sum_{n=1}^{N} e_n/(2m - 2n + 1);\ m = 1, 2, \ldots, N \quad (6)$$

where α_m is the angle or slope of the wing camber line at chord station m.

Received May 28, 1971.
Index categories: Subsonic and Transonic Flow; Airplane and Component Aerodynamics.

* Adjunct Professor, Department of Aerospace and Mechanical Engineering; also Consultant, Aerophysics Research Corp., Bellevue, Wash. Member AIAA.

Table 1

N/n	1	2	3	4	5	6
1	$\frac{1\times 1}{1}$					
2	$\frac{3\times 1}{2}$	$\frac{1\times 1}{2}$				
3	$\frac{5\times 3\times 1}{4\times 2}$	$\frac{3\times 1}{2\times 2}$	$\frac{3\times 1}{4\times 2}$			
4	$\frac{7\times 5\times 3\times 1}{6\times 4\times 2}$	$\frac{5\times 3\times 1}{4\times 2\times 2}$	$\frac{3\times 3\times 1}{2\times 4\times 2}$	$\frac{5\times 3\times 1}{6\times 4\times 2}$		
5	$\frac{9\times 7\times 5\times 3\times 1}{8\times 6\times 4\times 2}$	$\frac{7\times 5\times 3\times 1}{6\times 4\times 2\times 2}$	$\frac{5\times 3\times 1}{4\times 2\times 4\times 2}$	$\frac{3\times 5\times 3\times 1}{2\times 6\times 4\times 2}$	$\frac{7\times 5\times 3\times 1}{8\times 6\times 4\times 2}$	
6	$\frac{11\times 9\times 7\times 5\times 3\times 1}{10\times 8\times 6\times 4\times 2}$	$\frac{9\times 7\times 5\times 3\times 1}{8\times 6\times 4\times 2\times 2}$	$\frac{7\times 5\times 3\times 3\times 1}{6\times 4\times 2\times 4\times 2}$	$\frac{5\times 3\times 5\times 3\times 1}{4\times 2\times 6\times 4\times 2}$	$\frac{3\times 7\times 5\times 3\times 1}{2\times 8\times 6\times 4\times 2}$	$\frac{9\times 7\times 5\times 3\times 1}{10\times 8\times 6\times 4\times 2}$
↓	↓	↓	↓			↘
N	$\frac{(2N-1)!\text{ odd}}{(2N-2)!\text{ even}}$	$\frac{(2N-3)!\text{ odd}}{(2N-4)!\text{ even }2}$	$\frac{(2N-5)!\text{ odd }3!\text{ odd}}{(2N-6)!\text{ even }4!\text{ even}}$	.....	.....	$\frac{(2n-3)!\text{ odd}}{(2n-2)!\text{ even}}$

For the noncambered wing, $\alpha_m = \alpha$, then Eq. (6) becomes

$$\sum_{n=1}^{N} e_n/(2m - 2n + 1) = 1; \quad m = 1, 2, \ldots, N \qquad (7)$$

The solution of N linear simultaneous equations, gives the values of the chordwise additional loading, e_n.

A general solution of Eq. (7) for any value of N can be made by forming a mathematical series sequence of the loading terms as N increases. Equation (7) becomes for

$N = 1$, $e_1 = 1$

$N = 2$, $e_1 - e_2 = 1$; then $e_1 = \frac{3}{2}$

$(e_1/3) + e_2 = 1$ $e_2 = \frac{1}{2}$

$N = 3$, $e_1 - e_2 - (e_3/3) = 1$; then $e_1 = \frac{15}{8}$

$(e_1/3) + e_2 - e_3 = 1$ $e_2 = \frac{6}{8}$

$(e_1/5) + (e_2/3) + e_3 = 1$ $e_3 = \frac{3}{8}$

$N = 4$, $e_1 - e_2 - (e_3/3) - (e_4/5) = 1$; then $e_1 = \frac{35}{16}$

$(e_1/3) + e_2 - e_3 - (e_4/3) = 1$ $e_2 = \frac{15}{16}$

$(e_1/5) + (e_2/3) + e_3 - e_4 = 1$ $e_3 = \frac{9}{16}$

$(e_1/7) + (e_2/5) + (e_3/3) + e_4 = 1$ $e_4 = \frac{5}{16}$

This procedure is done for higher values of N until a mathematical sequence is formed as in Table 1. Inspection of these sequences determines the odd and even-factorial N row; and the N row in turn forms another sequence, so a general solution is given by

$$e_n = \frac{(2N - 2n + 1)!_{\text{odd}}(2n - 3)!_{\text{odd}}}{(2N - 2n)!_{\text{even}}(2n - 2)!_{\text{even}}} = \frac{(2N - 2n + 1)!(2n - 2)!}{2^{2N-2}[(N - n)!(n - 1)!]^2} \qquad (8)$$

The e_n values given by Eq. (8) is the solution of N simultaneous of Eq. (7), and N can be infinite.

With Eq. (5) inserted into Eq. (8), the chordwise vorticity is

$$\frac{\gamma_n}{V\alpha} = \frac{\pi(2N - 2n + 1)!(2n - 2)!}{2^{2N-2}[(N - n)!(n - 1)!]^2} \qquad (9)$$

Equation (9) gives the chordwise additional (or noncambered wing) loading in terms of circulation at N equal length panels or segments along the wing chord (see Fig. 1). The circulations are at the chordwise positions given by Eq. (2).

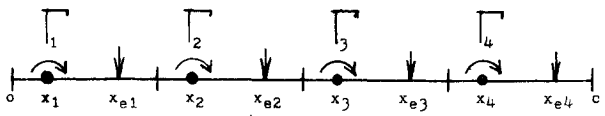

Fig. 1 The $\frac{1}{4}$ and $\frac{3}{4}$ points of each panel.

Solution for Infinite Panels

Equation (9) can be used to mathematically prove that finite element loading methods do converge on the exact answer as the number of elements are increased. Define $\xi_n = x_n/c$. Then, Eq. (2) can be written as

$$n = N\xi_n + \tfrac{3}{4} \qquad (10)$$

With Eq. (10) inserted into Eq. (9)

$$\frac{\gamma_n}{V\alpha} = \frac{\pi(2N - 2N\xi_n - \frac{1}{2})!(2N\xi_n - \frac{1}{2})!}{2^{2N-2}[(N - N\xi_n - \frac{3}{4})!(N\xi_n - \frac{1}{4})!]^2} \qquad (11)$$

As N becomes large

$$N! \to (2\pi)^{1/2}N^{N+1/2}e^{-N} \qquad (12)$$

Replacing the factorials in Eq. (11) by Eq. (12), then for large values of N

$$\frac{\gamma_n}{V\alpha} = 2\left[\frac{1 - \xi_n - \frac{3}{4}N^{-1}}{\xi_n - \frac{1}{4}N^{-1}}\right]^{1/2} \times \{1 + (2N)^{-1}[1 - \xi_n - \tfrac{3}{4}N^{-1}]^{-1/2}\} \qquad (13)$$

with N equal to infinity, Eq. (13) becomes

$$\gamma/V\alpha = 2[(1 - \xi)/\xi]^{1/2} \qquad (14)$$

where the subscripts n are removed since with infinite panels ξ is continuous.

Equation (14) is identical to that derived from thin-airfoil theory. With $\xi = \frac{1}{2}(1 - \cos\theta)$, the radical becomes the familiar cotangent loading. Thin-airfoil theory is part of aerodynamic literature (e.g., see the review given in Ref. 1).

Integration Accuracy and Factors for Chordwise Loading

Comparing with thin-airfoil theory, the lift-curve slope is given exactly for any N by twice the averaged value of $\gamma_n/V\alpha$. Thus, for $N = 3$, $c_{l\alpha} = \frac{2}{3}[(15\pi/8) + (3\pi/4) + (3\pi/8)] = 2\pi$. Likewise the moment is given exactly for any N. Besides for the chordwise cotangent loading, the lift and moment are summed exactly for the first and second sine harmonics of chordwise loading.

The discrete chordwise loading terms γ_n/V are constant over a given incremental chord distance c/N. For plotting the chordwise loading, γ_n/V is positioned at the quarter-chord of the nth segment, that is at $\xi_n = (n - \frac{3}{4})/N$. A chordwise loading factor can be formed that relates γ/V at ξ_n with γ_n/V. This factor defined by f_n is the ratio of thin-airfoil theory value, Eq. (14), to the incremental loading theory value, Eq. (9). Then

$$f_n = \frac{2^{2N-1}(N + \frac{3}{4} - n)^{1/2}[(N - n)!(n - 1)!]^2}{\pi(n - \frac{3}{4})^{1/2}(2N - 2n + 1)!(2n - 2)!} \qquad (15)$$

The loading at ξ_n is given by

$$\gamma/V = f_n(\gamma_n/V) \tag{16}$$

The factor f_n differs from unity primarily near the leading edge $n = 1$, and secondarily near the trailing edge $n = N$. For $N = 10$, f_n varies as

n	1	2	3	4	5
f_n	1.128	1.009	1.003	1.001	1.000
n	6	7	8	9	10
f_n	1.000	0.999	0.998	0.995	0.977

For other N values, f_1 varies as,

N	1	2	3	4	5	10	15
f_1	1.103	1.123	1.127	1.127	1.128	1.128	1.128

The f_n factors can be applied directly to finite aspect ratio lifting surface theories that are based on elemental horseshoe vortices, constant vorticity panels, or for multiple load and downwash lines as in Ref. 2. In Ref. 2, a 2-line loading theory is derived for a load-line which can be any arbitrary function of the lateral coordinate. A $2N$-line theory (N load lines, N downwash lines) is the superimposition of the 2-line theory along the chord, distributed as in Fig. 1. The circulation at each of the N load lines is factored by f_n to obtain the chordwise loading at ξ_n.

References

[1] DeYoung, J., "Analytical Camber for Leading-Edge Droop," Vought Rept. 2-53340/OR-50724, May 1970, LTV Aerospace Corp., Dallas, Texas.

[2] DeYoung, J., "Calculation of Span Loading for Arbitrary Plan Forms," *Journal of the Aeronautical Sciences*, Vol. 22, No. 3, March 1955, pp. 208–210.

Effect of Unsteady Pressure Gradient Reduction on Dynamic Stall Delay

FRANKLIN O. CARTA*
United Aircraft Research Laboratories, East Hartford, Conn.

Nomenclature

a = dimensionless pivot axis location in semichords, positive aft
C_p = unsteady pressure coefficient
C_{ps} = quasi-steady pressure coefficient
F = real part of Theodorsen function
G = imaginary part of Theodoresen function
k = reduced frequency, product of semichord and frequency divided by velocity
S = pressure gradient ratio
t = time, sec
x = dimensionless chord position in semichords, positive aft
α = pitch angle, positive nose up, rad or deg
ω = pitching frequency, rad/sec
$( )^*$ = complex quantity
$\overline{( )}$ = time-independent quantity

Introduction

THE unsteady dynamic stall phenomenon has been the subject of a number of recent investigations. Of particular interest is the apparent delay in stall on an airfoil moving through the steady-state stall regime with positive angular velocity. This has been observed whether the airfoil is oscillating harmonically[1–3] or increasing its angle of attack monotonically.[4,5]

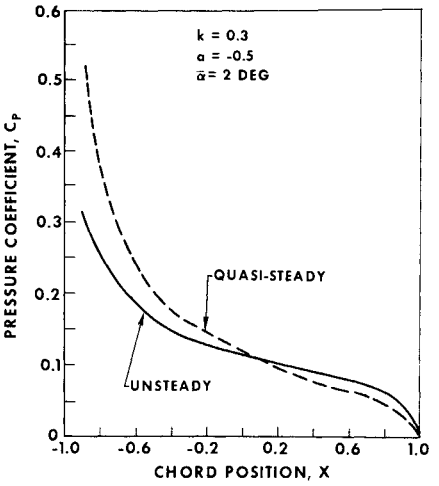

Fig. 1 Instantaneous pressure distribution at $\omega t = 11\pi/6$.

In a recent theoretical study Ham[6] was able to explain many of the features of moment reversal on an oscillating airfoil operating above the stall angle by postulating a continuously shed vortex sheet from the airfoil leading edge. However, he was unable to derive a criterion for the delay between the time the steady stall angle is exceeded and the time the vortex sheet begins to be shed. Isogai[7] has indicated that the delay is associated with the formation and movement of an unsteady separation bubble. However, one remaining unknown in his investigation is the way in which the separation bubble moves against the adverse pressure gradient without separating the boundary layer until well beyond the steady-state stall angle.

In this Note a possible theoretical mechanism for the delay in dynamic stall is discussed. The theory is confined to a comparison of the unsteady and quasi-steady chordwise potential flow pressure distributions. It is shown that the unsteady pressure gradient over the forward portion of the airfoil is less unfavorable than the steady pressure gradient. Hence, it can be inferred that a measurable stall margin exists for an unsteady motion relative to the steady state stalling angle, and that this stall margin increases with frequency.

Analysis

Theoretical pressure distributions

We can write the unsteady (or quasi-steady) pressure coefficient in the standard exponential form

$$C_p^* = \overline{C_p^*} e^{i\omega t} \tag{1}$$

where C_p is the pressure difference divided by the freestream dynamic pressure. The time-independent unsteady pressure coefficient, $\bar{C}_p^*$, for a pitching oscillation of amplitude $\bar{\alpha}$ is a complex function, reflecting the phase shift between pressure response and position. This is given by[8]

$$\bar{C}_p^* = 4\bar{\alpha}\{k^2[a - (x/2)](1 - x^2)^{1/2} + [F - kG(\tfrac{1}{2} - a)][(1 - x)/(1 + x)]^{1/2}\} + 4i\bar{\alpha}\{2k(1 - x^2)^{1/2} + [G + kF(\tfrac{1}{2} - a) - k/2][(1 - x)/(1 + x)]^{1/2}\} \tag{2}$$

where F and G are the real and imaginary parts of the Theodorsen function.[9] In the limit as $k \to 0$, Eq. (2) reduces to the quasi-steady form

$$\bar{C}_{p_s} = 4\bar{\alpha}[(1 - x)/(1 + x)]^{1/2} \tag{3}$$

It is assumed here that the motion is a harmonic function of time, given by

$$\alpha^* = \bar{\alpha} e^{i\omega t} \tag{4}$$

In an actual measurement on an oscillating airfoil the motion

Received May 24, 1971.
* Supervisor, Aeroelastics. Associate Fellow AIAA.